

# Learning Image Components for Object Recognition

**M. W. Spratling**

Division of Engineering, King’s College London. UK.

and Centre for Brain and Cognitive Development, Birkbeck College, London. UK.

## Abstract

In order to perform object recognition it is necessary to learn representations of the underlying components of images. Such components correspond to objects, object-parts, or features. Non-negative matrix factorisation is a generative model that has been specifically proposed for finding such meaningful representations of image data, through the use of non-negativity constraints on the factors. This article reports on an empirical investigation of the performance of non-negative matrix factorisation algorithms. It is found that such algorithms need to impose additional constraints on the sparseness of the factors in order to successfully deal with occlusion. However, these constraints can themselves result in these algorithms failing to identify image components under certain conditions. In contrast, a recognition model (a competitive learning neural network algorithm) reliably and accurately learns representations of elementary image features without such constraints.

**Keywords:** non-negative matrix factorisation; competitive learning; dendritic inhibition; object recognition

## 1 Introduction

An image usually contains a number of different objects, parts, or features and these components can occur in different configurations to form many distinct images. Identifying the underlying components which are combined to form images is thus essential for learning the perceptual representations necessary for performing object recognition. Non-negative matrix factorisation (NMF) has been proposed as a method for finding such parts-based decompositions of images (Lee and Seung, 1999; Feng et al., 2002; Liu et al., 2003; Liu and Zheng, 2004; Li et al., 2001; Hoyer, 2002, 2004). However, the performance of this method has not been rigorously or quantitatively tested. Instead, only a subjective assessment has been made of the quality of the components that are learnt when this method is applied to processing images of, for example, faces (Lee and Seung, 1999; Hoyer, 2004; Li et al., 2001; Feng et al., 2002). This paper thus aims to quantitatively test, using several variations of a simple standard test problem, the accuracy with which NMF identifies elementary image features. Furthermore, non-negative matrix factorisation assumes that images are composed of a linear combination of features. However, in reality the superposition of objects or object parts does not always result in a linear combination of sources but, due to occlusion, results in a non-linear combination. This paper thus also aims to investigate, empirically, how NMF performs when tested in more realistic environments where occlusion takes place. Since competitive learning algorithms have previously been applied to this test problem, and neural networks are a standard technique for learning object representations, the performance of NMF is compared to that of an unsupervised neural network learning algorithm applied to the same set of tasks.

## 2 Method

### 2.1 Non-Negative Matrix Factorisation

Given an  $m$  by  $p$  matrix  $\mathbf{X} = [\vec{x}_1, \dots, \vec{x}_p]$ , each column of which contains the pixel values of an image (*i.e.*,  $\mathbf{X}$  is a set of training images), the aim is to find the factors  $\mathbf{A}$  and  $\mathbf{Y}$  such that:

$$\mathbf{X} \approx \mathbf{A}\mathbf{Y}$$

Where  $\mathbf{A}$  is an  $m$  by  $n$  matrix the columns of which contain basis vectors, or components, into which the images can be decomposed, and  $\mathbf{Y} = [\vec{y}_1, \dots, \vec{y}_p]$  is an  $n$  by  $p$  matrix containing the activations of each component (*i.e.*, the strength of each basis vector in the corresponding training image). A training image ( $\vec{x}_k$ ) can therefore be reconstructed as a linear combination of the image components contained in  $\mathbf{A}$ , such that  $\vec{x}_k \approx \mathbf{A}\vec{y}_k$ .

A number of different learning algorithms can be defined depending on the constraints that are placed on the factors  $\mathbf{A}$  and  $\mathbf{Y}$ . For example, vector quantization (VQ) restricts each column of  $\mathbf{Y}$  to have only one non-zero element, principal components analysis (PCA) constrains the columns of  $\mathbf{A}$  to be orthonormal and the rows of  $\mathbf{Y}$

	Acronym	Description	Reference
Non-negative Matrix Factorisation Algorithms	nmfdiv	NMF with divergence objective	(Lee and Seung, 2001)
	nmfmse	NMF with euclidean objective	(Lee and Seung, 2001)
	lnmf	Local NMF	(Li et al., 2001; Feng et al., 2002)
	snmf	Sparse NMF ( $\alpha = 1$ )	(Liu et al., 2003)
	nnscc	Non-negative sparse coding ( $\lambda = 1$ )	(Hoyer, 2002)
	nmfsc (A)	NMF with a sparseness constraint of 0.5 on the basis vectors	(Hoyer, 2004)
	nmfsc (Y)	NMF with a sparseness constraint of 0.7 on the activations	(Hoyer, 2004)
	nmfsc (A&Y)	NMF with sparseness constraints of 0.5 on the basis vectors and 0.7 on the activations	(Hoyer, 2004)
Neural Network Algorithms	nndi	Dendritic inhibition neural network with non-negative weights	
	di	Dendritic inhibition neural network	(Spratling and Johnson, 2002, 2003)

**Table 1:** The algorithms tested in this article. These include a number of different algorithms for finding matrix factorisations under non-negativity constraints and a neural network algorithm for performing competitive learning through dendritic inhibition.

to be mutually orthogonal, and independent components analysis (ICA) constrains the rows of  $\mathbf{Y}$  to be statistically independent. Non-negative matrix factorisation is a method that seeks to find factors (of a non-negative matrix  $\mathbf{X}$ ) under the constraint that both  $\mathbf{A}$  and  $\mathbf{Y}$  contain only elements with non-negative values. It has been proposed that this method is particularly suitable for finding the components of images, since from the physical properties of image formation it is known that image components are non-negative and that these components are combined additively (*i.e.*, are not subtracted) in order to generate images. Several different algorithms have been proposed for finding the factors  $\mathbf{A}$  and  $\mathbf{Y}$  under non-negativity constraints. Those tested here are listed in Table 1.

Algorithms `nmfdiv` and `nmfmse` impose non-negativity constraints solely, and differ only in the objective function that is minimised in order to find the factors. All the other algorithms extend non-negative matrix factorisation by imposing additional constraints on the factors. Algorithm `lnmf` imposes constraints that require the columns of  $\mathbf{A}$  to contain as many non-zero elements as possible, and  $\mathbf{Y}$  to contain as many zero elements as possible. This algorithm also requires that basis vectors be orthogonal. Both algorithms `snmf` and `nnscc` impose constraints on the sparseness of  $\mathbf{Y}$ . Algorithm `nmfsc` allows optional constraints to be imposed on the sparseness of either the basis vectors, the activations, or both. This algorithm was used with three combinations of sparseness constraints. For `nmfsc (A)` a constraint on the sparseness of the basis vectors was applied. This constraint required that each column of  $\mathbf{A}$  had a sparseness of 0.5. Valid values for the parameter controlling sparseness could range from 0 (which would produce completely distributed basis vectors) to a value of 1 (which would produce completely sparse basis vectors). For `nmfsc (Y)` a constraint on the sparseness of the activations was applied. This constraint required that each row of  $\mathbf{Y}$  had a sparseness of 0.7 (where sparseness is in the range  $[0, 1]$ , as for the constraint on  $\mathbf{A}$ ). For `nmfsc (A&Y)` these same constraints were imposed on both the sparseness of basis vectors and the activations. For the `nmfsc` algorithm, fixed values for the parameters controlling sparseness were used in order to provide a fairer comparison with the other algorithms all of which used constant parameter settings. Furthermore, since all the test cases studied are very similar, it is reasonable to expect an algorithm to work across them all without having to be tuned specifically to each individual task. The particular parameter values used were selected so as to provide the best overall results across all the tasks. The effect of changing the sparseness parameters is described in the discussion section.

## 2.2 Dendritic Inhibition Neural Network

In terms of neural networks, the factoring of  $\mathbf{X}$  into  $\mathbf{A}$  and  $\mathbf{Y}$  constitutes the formation of a generative model (Hinton et al., 1995): neural activations  $\mathbf{Y}$  reconstruct the input patterns  $\mathbf{X}$  via a matrix of feedback (or generative)

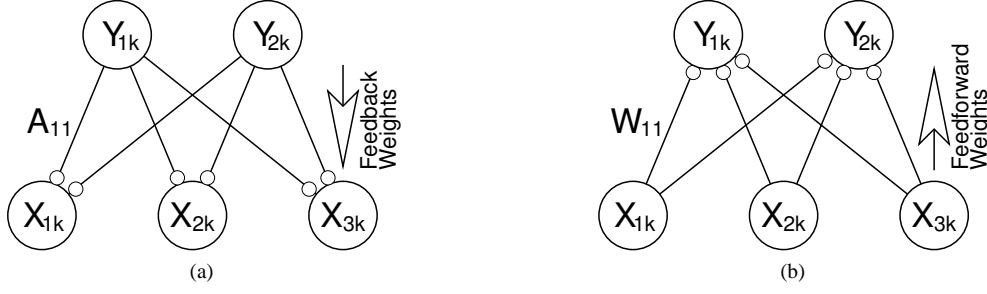


**Figure 1:** (a) A generative neural network model: feedback connections enable neural activations ( $\vec{y}_k$ ) to reconstruct an input pattern ( $\vec{x}_k$ ). (b) A recognition neural network model: feedforward connections cause neural activations ( $\vec{y}_k$ ) to be generated in response to an input pattern ( $\vec{x}_k$ ). Nodes are shown as large circles and excitatory synapses as small open circles.

synaptic weights  $\mathbf{A}$  (see Figure 1a). In contrast, traditional neural network algorithms have attempted to learn a set of feedforward (recognition) weights  $\mathbf{W}$  (see Figure 1b), such that:

$$\mathbf{Y} = f(\mathbf{W}, \mathbf{X})$$

Where  $\mathbf{W}$  is an  $n$  by  $m$  matrix of synaptic weight values,  $\mathbf{X} = [\vec{x}_1, \dots, \vec{x}_p]$  is an  $m$  by  $p$  matrix of training images, and  $\mathbf{Y} = [\vec{y}_1, \dots, \vec{y}_p]$  is an  $n$  by  $p$  matrix containing the activation of each node in response to the corresponding image. Typically, the rows of  $\mathbf{W}$  form templates that match image features, so that individual nodes become active in response to the presence of specific components of the image. Nodes thus act as ‘feature detectors’ (Barlow, 1990, 1995).

Many different functions are possible for calculating neural activations and many different learning rules can be defined for finding the values of  $\mathbf{W}$ . For example, algorithms have been proposed for performing vector quantization (Kohonen, 1997; Ahalt et al., 1990), principal components analysis (Oja, 1992; Fyfe, 1997b; Földiák, 1989), and independent components analysis (Jutten and Herault, 1991; Charles and Fyfe, 1997; Fyfe, 1997a). Many of these algorithms impose non-negativity constraints on the elements of  $\mathbf{Y}$  and  $\mathbf{W}$  for reasons of biological plausibility, since neural firing rates are positive and since synapses can not change between being excitatory and being inhibitory. In general, such algorithms employ different forms of competitive learning, in which nodes compete to be active in response to each input pattern. Such competition can be implemented using a number of different forms of lateral inhibition. In this paper, a competitive learning algorithm in which nodes can inhibit the inputs to other nodes is used. This form of inhibition has been termed dendritic inhibition or pre-integration lateral inhibition. The full dendritic inhibition model (Spratling and Johnson, 2002, 2003) allows negative synaptic weight values. However, in order to make a fairer comparison with NMF, a version of the dendritic inhibition algorithm in which all synaptic weights are restricted to be non-negative (by clipping the weights at zero) is also used in the experiments described here. The full model will be referred to by the acronym di while the non-negative version will be referred to as nndi (see Table 1).

In a neural network model, an input image ( $\vec{x}_k$ ) generates activity ( $\vec{y}_k$ ) in the nodes of a neural network such that  $\vec{y}_k = f(\mathbf{W}, \vec{x}_k)$ . In the dendritic inhibition model, the activation of each individual node is calculated as:

$$y_{jk} = \mathbf{W} \vec{x}'_{kj}$$

where  $\vec{x}'_{kj}$  is an inhibited version of the input activations ( $\vec{x}_k$ ) that can differ for each node. The values of  $\vec{x}'_{kj}$  are calculated as:

$$x'_{ikj} = x_{ik} \left( 1 - \alpha \max_{\substack{r=1 \\ (r \neq j)}}^n \left\{ \frac{w_{ri}}{\max_{q=1}^m \{w_{rq}\}} \frac{y_{rk}}{\max_{q=1}^n \{y_{qk}\}} \right\} \right)^+.$$

Where  $\alpha$  is a scale factor controlling the strength of lateral inhibition, and  $(v)^+$  is the positive half-rectified value of  $v$ . The steady-state values of  $y_{jk}$  were found by iteratively applying the above two equations, increasing the value of  $\alpha$  from 0 to 6 in steps of 0.25, while keeping the input image fixed.

The above activation function implements a form of lateral inhibition in which each neuron can inhibit the inputs to other neurons. The strength with which a node inhibits an input to another node is proportional to the strength of the afferent weight the inhibiting node receives from that particular input. Hence, if a node is strongly activated by the overall stimulus and it has a strong synaptic weight to a certain feature of that stimulus, then it will

inhibit other nodes from responding to that feature. On the other hand, if an active node receives a weak weight from a feature then it will only weakly inhibit other nodes from responding to that feature. In this manner, each node can selectively ‘block’ its preferred inputs from activating other nodes, but does not inhibit other nodes from responding to distinct stimuli.

All weight values were initialised to random values chosen from a Gaussian distribution with a mean of  $\frac{1}{m}$  and a standard deviation of  $0.001 \frac{n}{m}$ . This small degree of noise on the initial weight values was sufficient to cause bifurcation of the activity values, and thus to cause differentiation of the receptive fields of different nodes through activity-dependent learning. Previous results with this algorithm have been produced using noise (with a similarly small magnitude) applied to the node activation values. Using noise applied to the node activations, rather than the weights, produces similar results to those reported in this article. However, noise was only applied to the initial weight values, and not to the node activations, here to provide a fairer comparison to the deterministic NMF algorithms. Note that a node which still has its initial weight values (*i.e.*, a node which has not had its weights modified by learning) is described as ‘uncommitted’.

Synaptic weights were adjusted using the following learning rule (applied to weights with values greater than or equal to zero):

$$\Delta w_{ji} = \frac{(x_{ik} - \bar{x}_k)}{\sum_{p=1}^m x_{pk}} (y_{jk} - \bar{y}_k)^+ \quad (1)$$

Where  $\bar{x}_k$  is the mean value of the pixels in the training image (*i.e.*,  $\bar{x}_k = \frac{1}{m} \sum_{i=1}^m x_{ik}$ ), and  $\bar{y}_k$  is the mean of the output activations (*i.e.*,  $\bar{y}_k = \frac{1}{n} \sum_{j=1}^n y_{jk}$ ). Following learning, synaptic weights were clipped at zero such that  $w_{ji} = (w_{ji})^+$  and were normalised such that  $\sum_{i=1}^m (w_{ji})^+ \leq 1$ .

This learning rule encourages each node to learn weights selective for a set of coactive inputs. This is achieved since when a node is more active than average it increases its synaptic weights to active inputs and decreases its weights to inactive inputs. Hence, only sets of inputs which are consistently coactive will generate strong afferent weights. In addition, the learning rule is designed to ensure that different nodes can represent stimuli which share input features in common (*i.e.*, to allow the network to represent overlapping patterns). This is achieved by rectifying the post-synaptic term of the rule so that no weight changes occur when the node is less active than average. If learning was not restricted in this way, whenever a pattern was presented all nodes which represented patterns with overlapping features would reduce their weights to these features.

For the algorithm `di`, but not for algorithm `nndi`, the following learning rule was applied to weights with values less than or equal to zero:

$$\Delta w_{ji} = \frac{(x'_{ikj} - 0.5x_{ik})^-}{\sum_{p=1}^n y_{pk}} (y_{jk} - \bar{y}_k) \quad (2)$$

Where  $(v)^-$  is the negative half-rectified value of  $v$ . Negative weights were clipped at zero such that  $w_{ji} = (w_{ji})^-$  and were normalised such that  $\sum_{i=1}^m (w_{ji})^- \geq -1$ . Note that for programming convenience a single synapse is allowed to take either excitatory or inhibitory weight values. In a more biologically plausible implementation two separate sets of afferent connections could be used: the excitatory ones being trained using equation 1 and the inhibitory ones being trained using a rule similar to equation 2.

The negative weight learning rule has a different form from the positive weight learning rule as it serves a different purpose. The negative weights are used to ensure that each image component is represented by a distinct node rather than by the partial activation of multiple nodes each of which represents an overlapping image component. A full explanation of this learning rule is provided together with a concrete example of its function in section 3.3.

### 3 Results

In each of the experiments reported below, all the algorithms listed in Table 1 were applied to learning the components in a set of  $p$  training images. The average number of components that were correctly identified over the course of 25 trials was recorded. A new set of  $p$  randomly generated images were created for each trial. In each trial the NMF algorithms were trained until the total sum of the absolute difference in the objective function, between successive epochs, had not changed by more than 0.1% of its average value in 100 epochs, or until 2000 epochs had been completed. One epoch is when the method has been trained on all  $p$  training patterns. Hence, an epoch equals one update to the factors in an NMF algorithm, and  $p$  iterations of the neural network algorithm during which each individual image in the training set is presented once as input to the network. The neural network algorithms were trained for 10000 iterations. Hence, the NMF algorithms were each trained for at least 100

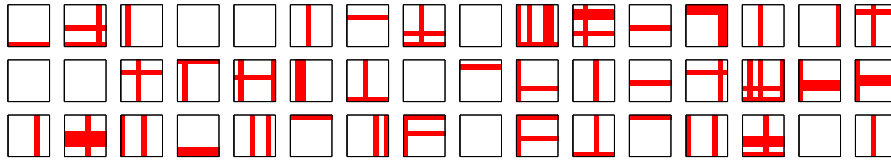


**Figure 2:** Typical training patterns for the standard bars problem. Horizontal and vertical bars in 8x8 pixel images are independently selected to be present with a probability of  $\frac{1}{8}$ . Dark pixels indicate active inputs.

epochs, while the neural network algorithms were trained for at most 100 epochs (since the value of  $p$  was 100 or greater).

### 3.1 Standard Bars Problem

The bars problem (and its variations) is a benchmark task for the learning of independent image features (Földiák, 1990; Saund, 1995; Dayan and Zemel, 1995; Hinton et al., 1995; Harpur and Prager, 1996; Hinton and Ghahramani, 1997; Frey et al., 1997; Fyfe, 1997b; Charles and Fyfe, 1998; Hochreiter and Schmidhuber, 1999; Meila and Jordan, 2000; Plumbley, 2001; O’Reilly, 2001; Ge and Iwata, 2002; Lücke and von der Malsburg, 2004). In the standard version of the bars problem, as defined by Földiák (1990), training data consists of 8 by 8 pixel images in which each of the 16 possible (one-pixel wide) horizontal and vertical bars can be present with a probability of  $\frac{1}{8}$ . Typical examples of training images are shown in Figure 2.

In the first experiment the algorithms were trained on the standard bars problem. Twenty-five trials were performed with  $p = 100$ , and, with  $p = 400$ . The number of components that each algorithm could learn ( $n$ ) was set to 32. Typical examples of the (generative) weights learnt by each NMF algorithm (*i.e.*, the columns of  $\mathbf{A}$  reshaped as 8 by 8 pixel images) and of the (recognition) weights learnt by the neural network algorithms (*i.e.*, the rows of  $\mathbf{W}$  reshaped as 8 by 8 pixel images) are shown in Figure 3. It can be seen that the NMF algorithms tend to learn a redundant representation, since the same bar can be represented multiple times. In contrast, the neural network algorithms learnt a much more compact code, with each bar being represented by a single node. It can also be seen that many of the NMF algorithms learnt representations of bars in which pixels were missing. Hence, these algorithms learnt random pieces of image components rather than the image components themselves. In contrast, the neural network algorithms (and algorithms  $\text{nmsc}$ ,  $\text{nmfsc}(\mathbf{A})$ , and  $\text{nmfsc}(\mathbf{A\&Y})$ ) learnt to represent complete image components.

To quantify the results, the following procedure was used to determine the number of bars represented by each algorithm in each trial. For each node, the sum of the weights corresponding to each row and column of the input image was calculated. A node was considered to represent a particular bar if the total weight corresponding to that bar was twice that of the sum of the weights for any other row or column and if the minimum weight in the row or column corresponding to that bar was greater than the mean of all the (positive) weights for that node. The number of unique bars represented by at least one basis vector, or one node of the network, was calculated, and this value was averaged over the 25 trials. The mean number of bars (*i.e.*, image components) represented by each algorithm is shown in Figure 4a. Good performance requires both accuracy (finding all the image components) and reliability (doing so across all trials). Hence, the average number of bars represented needs to be close to 16 for an algorithm to be considered to have performed well. It can be seen that when  $p = 100$ , most of the NMF algorithms performed poorly on this task. However, algorithms  $\text{nmfsc}(\mathbf{A})$  and  $\text{nmfsc}(\mathbf{A\&Y})$  produced good results, representing an average of 15.7 and 16 components respectively. This compares favourably to the neural network algorithms, with  $\text{nndi}$  representing 14.6 and  $\text{di}$  representing 15.9 of the 16 bars. When the number of images in the training set was increased to 400 this improved the performance of certain NMF algorithms, but lead to worse performance in others. For  $p = 400$ , every image component in every trial was found by algorithms  $\text{nmsc}$ ,  $\text{nmfsc}(\mathbf{A})$ ,  $\text{nmfsc}(\mathbf{A\&Y})$  and  $\text{di}$ .

In the previous experiment there were significantly more nodes, or basis vectors, than was necessary to represent the 16 underlying image components. The poor performance of certain algorithms could thus potentially be due to over-fitting. The experiment was thus repeated using 16 nodes or basis vectors. The results of this experiment are shown in Figure 4b. It can be seen that while the performance of some NMF algorithms is improved, the performance of others becomes slightly worse. Only NMF algorithms  $\text{nmfsc}(\mathbf{A})$  and  $\text{nmfsc}(\mathbf{A\&Y})$  reliably find nearly all the bars with both 16 and 32 basis vectors. In contrast, the performance of the neural network algorithms is unaffected by changing the number of nodes. Such behaviour is desirable since it is generally not known in advance how many components there are. Hence, a robust algorithm needs to be able to correctly learn

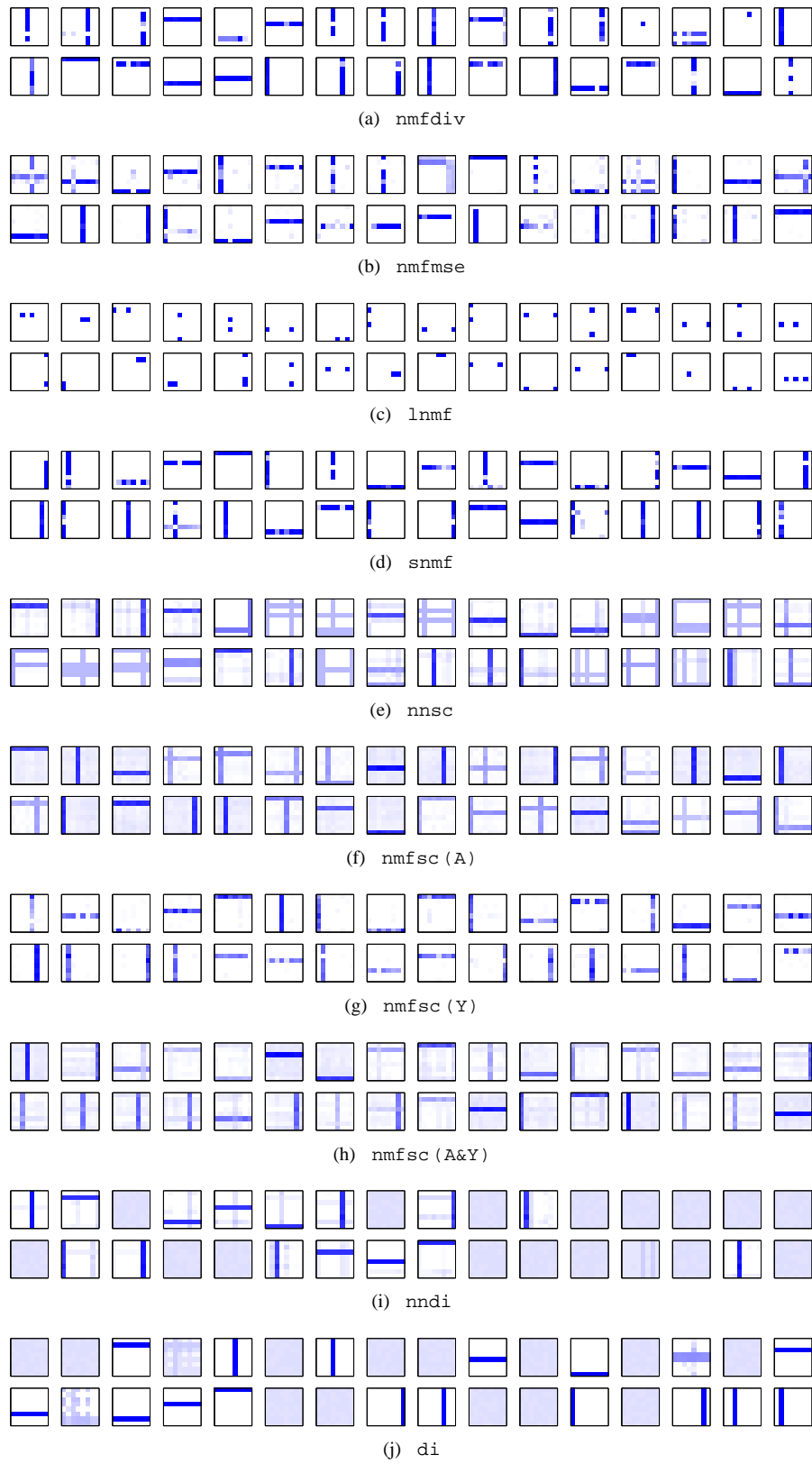
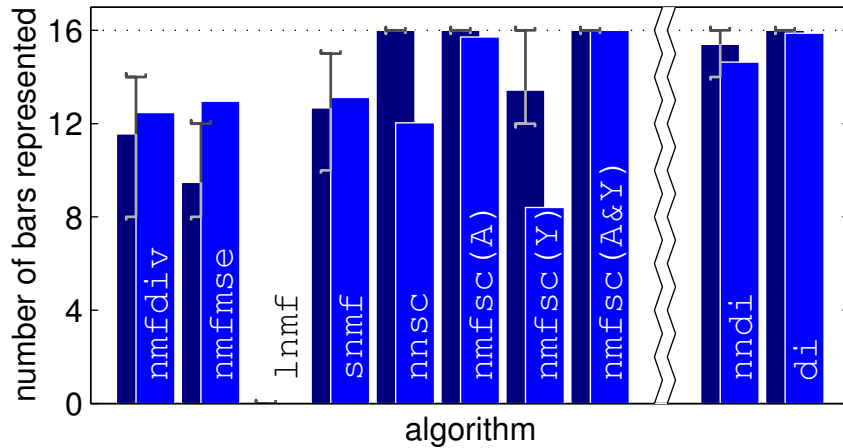
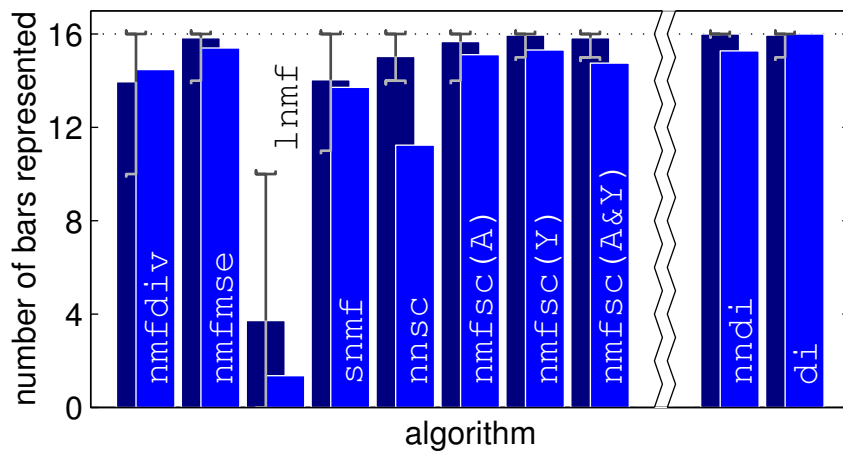


**Figure 3:** Typical generative or recognition weights learnt by 32 basis vectors or nodes when each algorithm was trained on the standard bars problem. Dark pixels indicate strong weights.



(a)



(b)

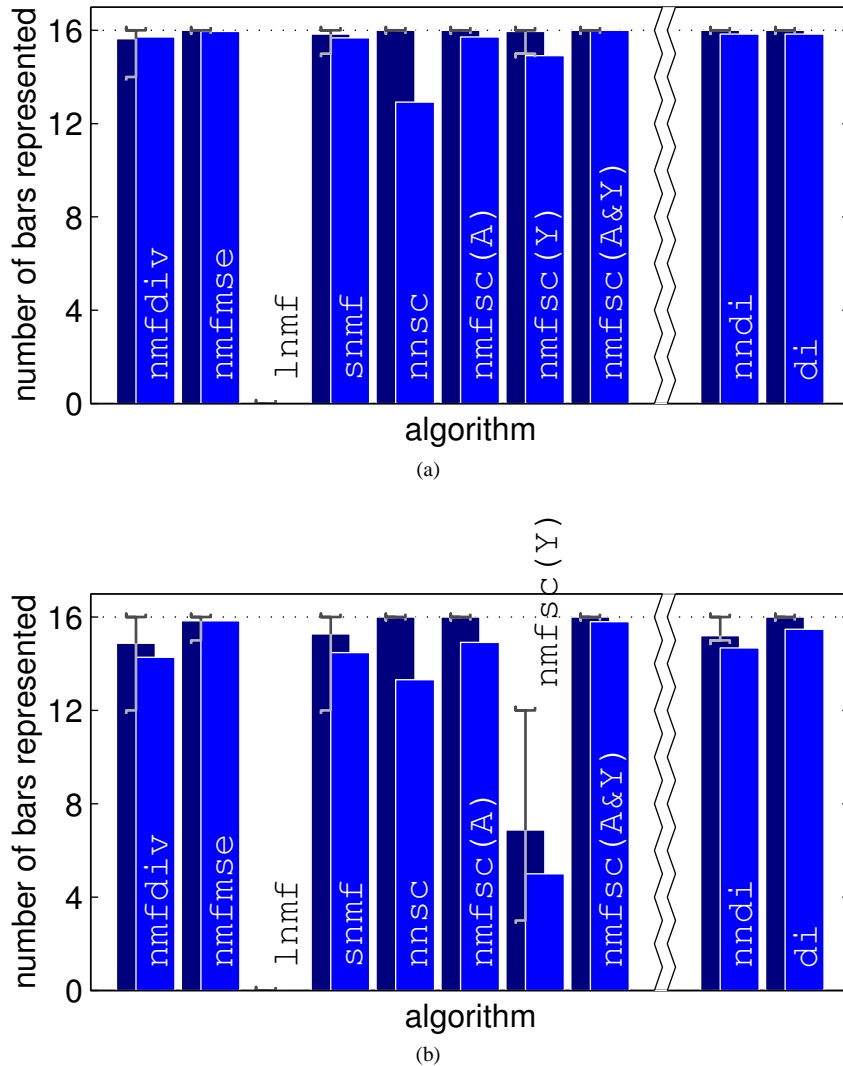
**Figure 4:** Performance of each algorithm when trained on the standard bars problem. For (a) 32, and (b) 16 basis vectors or nodes. Each bar shows the mean number of components correctly identified by each algorithm when tested over 25 trials. Results for different training set sizes are shown: the lighter, foreground, bars show results for  $p = 100$ , and the darker, background, bars show results for  $p = 400$ . Error bars show best and worst performance, across the 25 trials, when  $p = 400$ .

image components with an excess of nodes. Across both these experiment the `di` version of the neural network algorithm performs as well as or better than any of the NMF algorithms.

### 3.2 Bars Problems Without Occlusion

To determine the effect of occlusion on the performance of each algorithm further experiments were performed using versions of the bars problem in which no occlusion occurs. Firstly, a linear version of the standard bars problem was used. Similar tasks have been used by [Plumbley \(2001\)](#) and [Hoyer \(2002\)](#). In this task, pixel values are combined additively at points of overlap between horizontal and vertical bars. As with the standard bars problem, training data consisted of 8 by 8 pixel images in which each of the 16 possible (one-pixel wide) horizontal and vertical bars could be present with a probability of  $\frac{1}{8}$ . All the algorithms were trained with  $p = 100$  and with  $p = 400$  using 32 nodes or basis vectors. The number of unique bars represented by at least one basis vector, or one node of the network, was calculated, and this value was averaged over 25 trials. The mean number of bars represented by each algorithm is shown in Figure 5a.

Another version of the bars problem in which occlusion is avoided is one in which horizontal and vertical bars do not co-occur. Similar tasks have been used by [Hinton et al. \(1995\)](#); [Dayan and Zemel \(1995\)](#); [Frey et al. \(1997\)](#); [Hinton and Ghahramani \(1997\)](#) and [Meila and Jordan \(2000\)](#). In this task, an orientation (either horizontal or vertical) was chosen with equal probability for each training image. The eight (one-pixel wide) bars of that orientation were then independently selected to be present with a probability of  $\frac{1}{8}$ . All the algorithms were trained



**Figure 5:** Performance of each algorithm when trained on (a) the linear bars problem, and (b) the one-orientation bars problem, with 32 basis vectors or nodes. Each bar shows the mean number of components correctly identified by each algorithm when tested over 25 trials. Results for different training set sizes are shown: the lighter, foreground, bars show results for  $p = 100$ , and the darker, background, bars show results for  $p = 400$ . Error bars show best and worst performance, across the 25 trials, when  $p = 400$ .

with  $p = 100$  and with  $p = 400$  using 32 nodes or basis vectors. The number of unique bars represented by at least one basis vector, or one node of the network, was calculated, and this value was averaged over 25 trials. The mean number of bars represented by each algorithm is shown in Figure 5b.

For both experiments using training images in which occlusion does not occur, the performance of most of the NMF algorithms is improved considerably in comparison to the standard bars problem. The neural network algorithms also reliably learn the image components as with the standard bars problem.

### 3.3 Bars Problem With More Occlusion

To further explore the effects of occlusion on the learning of image components a version of the bars problem with double-width bars was used. Training data consisted of 9 by 9 pixel images in which each of the 16 possible (two-pixel wide) horizontal and vertical bars could be present with a probability  $\frac{1}{8}$ . The image size was increased by one pixel to keep the number of image components equal to 16 (as in the previous experiments). In this task, as in the standard bars problem, perpendicular bars overlap; however, the proportion of overlap is increased. Furthermore, neighbouring parallel bars also overlap (by 50%). Typical examples of training images are shown in Figure 6.

Each algorithm was trained on this double-width bars problem with  $p = 400$ . The number of components that

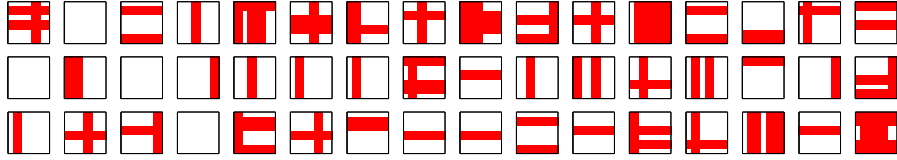


**Figure 6:** Typical training patterns for the double-width bars problem. Two pixel wide horizontal and vertical bars in a 9x9 pixel image are independently selected to be present with a probability of  $\frac{1}{8}$ . Dark pixels indicate active inputs.

each algorithm could learn ( $n$ ) was set to 32. Typical examples of the (generative) weights learnt by each NMF algorithm and of the (recognition) weights learnt by the neural network algorithms are shown in Figure 7. It can be seen that the majority of the NMF algorithms learnt redundant encodings in which the basis vectors represent parts of image components rather than complete components. In contrast, the neural network algorithms (and the `nnsC` algorithm) learnt to represent complete image components.

The following procedure was used to determine the number of bars represented by each algorithm in each trial. For each node, the sum of the weights corresponding to every double-width bar was calculated. A node was considered to represent a particular bar if the total weight corresponding to that bar was 1.5 times that of the sum of the weights for any other bar and if the minimum weight of any pixel forming part of that bar was greater than the mean of all the (positive) weights for that node. The number of unique bars represented by at least one basis vector, or one node of the network, was calculated. The mean number of two-pixel-wide bars, over the 25 trials, represented by each algorithm is shown in Figure 8a. This set of training images could be validly, but less efficiently, represented by 18 one-pixel-wide bars. Hence, the mean number of one-pixel-wide bars, represented by each algorithm was also calculated and this data is shown in Figure 8b. The number of one-pixel-wide bars represented was calculated using the same procedure used to analyse the previous results (as stated in section 3.1).

It can be seen that the majority of the NMF algorithms perform very poorly on this task. Most fail to reliably represent either double- or single-width bars. However, algorithms `nnsC`, `nmfSC (A)` and `nmfSC (A&Y)` do succeed in learning the image components. The dendritic inhibition algorithm, with negative weights, also succeeds in identifying all the double-width bars in most trials. However, the non-negative version of this algorithm performs less well. This result illustrates the need to allow negative weight values in this algorithm in order to robustly learn image components. Negative weights are needed to disambiguate a real image component from the simultaneous presentation of partial components. For example, consider part of the neural network that is receiving input from four pixels that are part of four separate, neighbouring, columns of the input image (as illustrated in Figure 9). Assume that two nodes in the output layer (nodes 1 and 3) have learnt weights that are selective to two neighbouring, but non-overlapping, double-width bars (bars 1 and 3). When the double-width bar (bar 2) that overlaps these two represented bars is presented to the input, then the network will respond by partially activating nodes 1 and 3. Such a representation is reasonable since this input pattern could be the result of the co-activation of partially occluded versions of the two represented bars. However, if bar 2 recurs frequently then it is unlikely to be caused by the chance co-occurrence of multiple, partially occluded patterns, and is more likely to be an independent image component that should be represented in a similar way to the other components (*i.e.*, by the activation of a specific node tuned to that feature). One way to ensure that in such situations the network learns all image components is to employ negative synaptic weights. These negative weights are generated when a node is active and inputs, which are not part of the nodes' preferred input pattern, are inhibited. This can only occur when multiple nodes are co-active. If the pattern, to which this set of co-active nodes are responding, re-occurs then the negative weights will grow. When the negative weights are sufficiently large the response of these nodes to this particular pattern will be inhibited, enabling an uncommitted node to successfully compete to represent this pattern. On the other hand, if the pattern, to which this set of co-active nodes are responding, is just due to the co-activation of independent input patterns then the weights will return toward zero on subsequent presentations of these patterns in isolation.

### 3.4 Bars Problem with Unequal Components

In each individual experiment reported in the previous sections, every component of the training images has been exactly equal in size to every other component and has occurred with exactly the same probability. This is unlikely to be the case in real-world object recognition tasks. In the real-world, different image features can be radically different in size and can be encountered with very different frequency. For example, important features in face recognition include both the eyes and the hair (Sinha and Poggio, 1996; Davies et al., 1979) which can vary

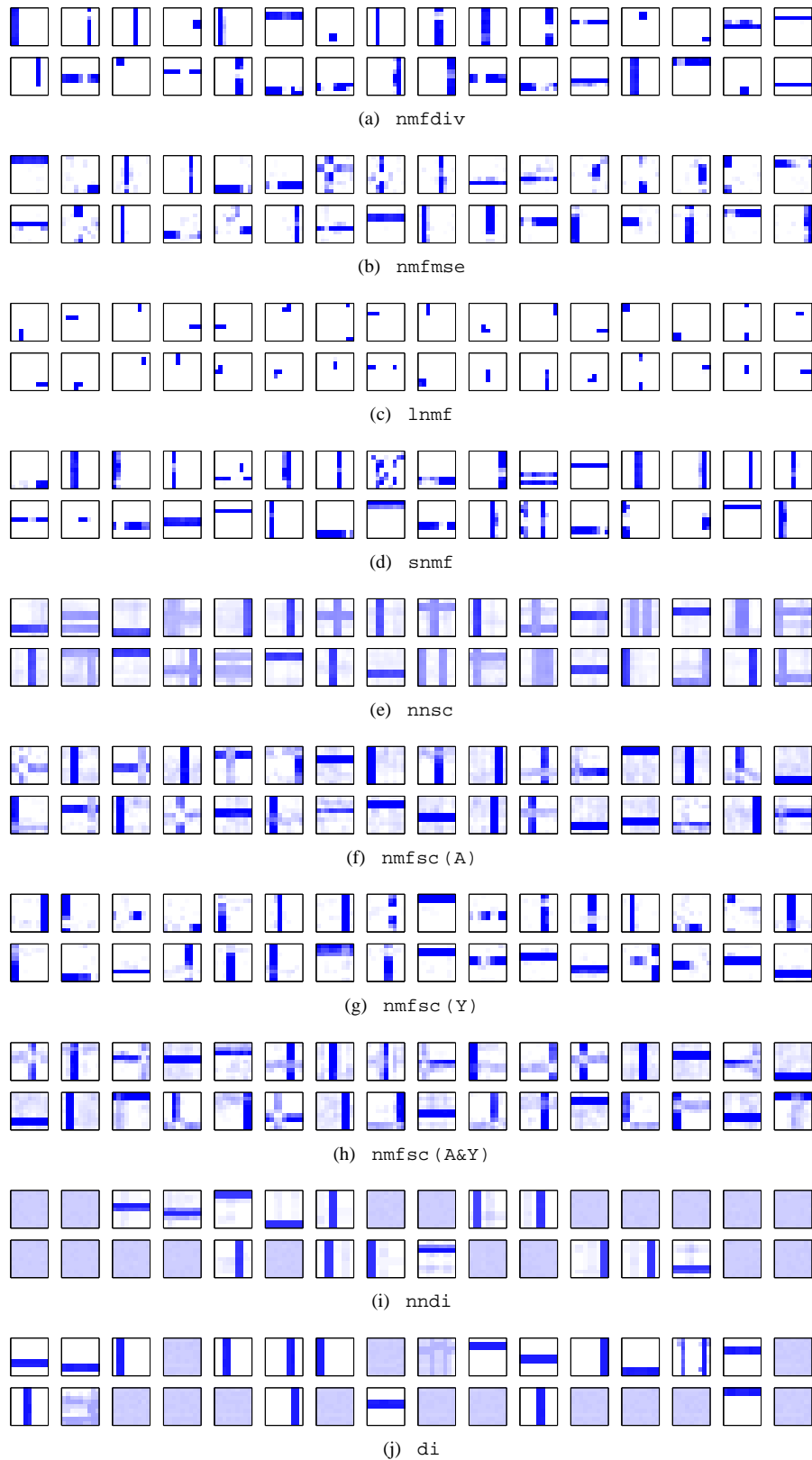
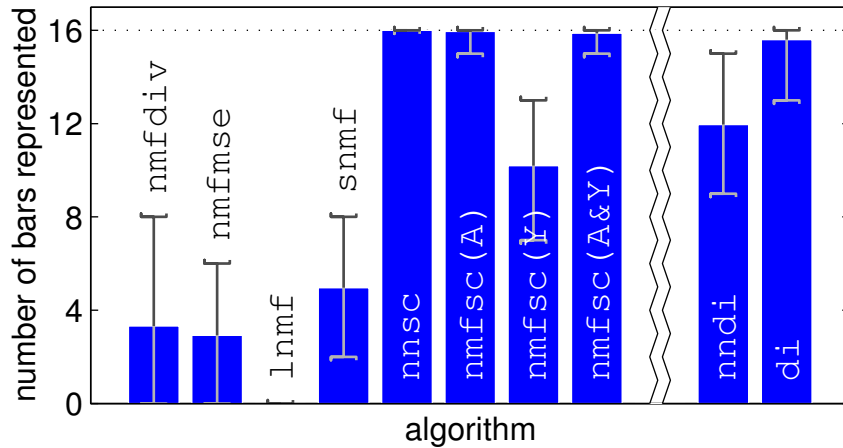
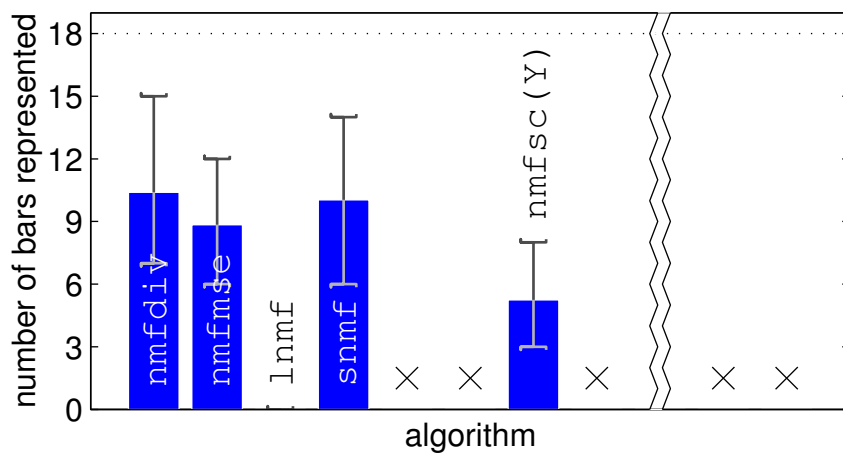


**Figure 7:** Typical generative or recognition weights learnt by 32 basis vectors or nodes when each algorithm was trained on the double-width bars problem. Dark pixels indicate strong weights.



(a)



(b)

**Figure 8:** Performance of each algorithm when trained on the double-width bars problem, with 32 basis vectors or nodes, and  $p = 400$ . Each bar shows the mean number of components correctly identified by each algorithm when tested over 25 trials. (a) Number of double-width bars learnt. (b) Number of single-width bars learnt. Error bars show best and worst performance across the 25 trials. Note that algorithms that successfully learnt double-width bars - see (a) - do not appear in (b), but space is left for these algorithms in order to aid comparison between figures.

significantly in relative size. Furthermore, we effortlessly learn to recognise both immediate family members (who may be seen many times a day) and distant relatives (who may be seen only a few times a year).

To provide a more realistic test, a new variation on the bars problem was used. In this version, training data consisted of 16 by 16 pixel images. Image components consisted of seven one-pixel wide bars and one nine-pixel wide bar in both the horizontal and vertical directions. Hence, as in previous experiments, there were eight image components at each orientation and 16 in total. Parallel bars did not overlap, however, the proportion of overlap between the nine-pixel wide bars and all other perpendicular bars was large, while the proportion of overlap between perpendicular one-pixel wide bars was less than in the standard bars problem. Each horizontal bar was selected to be present in an image with a probability of  $\frac{1}{8}$  while vertical bars occurred with a probability of  $\frac{1}{32}$ . Hence, in this test case half the underlying image components occurred at a different frequency to the other half and two of the components were a different size to the other 14.

Each algorithm was trained on this ‘unequal’ bars problem with  $p = 400$ . The number of components that each algorithm could learn ( $n$ ) was set to 32. The mean number of bars, over 25 trials, represented by each algorithm is shown in Figure 10. It can be seen that none of the NMF algorithms succeeded in reliably identifying all the image components in this task. Learning to represent the two large components appears to be a particular problem for all these algorithms, but the cause for this may differ between algorithms. For most NMF algorithms, the underlying linear model fails when occlusion is significant, as is the case for the two nine-pixel wide patterns. However, for the NMF algorithms that find non-negative factors with an additional constraint on the sparseness of

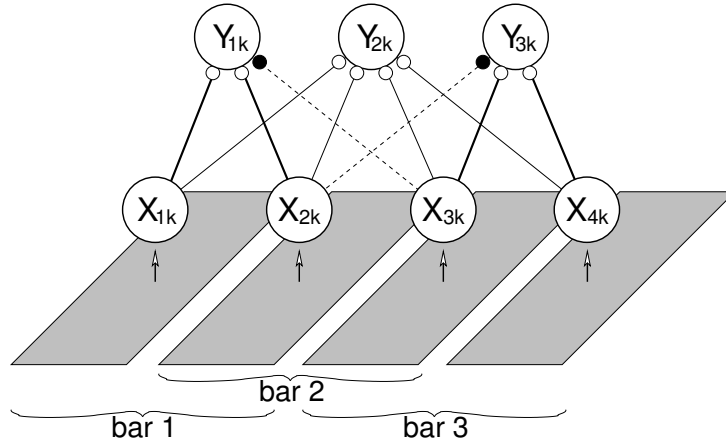


**Figure 9:** An illustration of the role of negative weights in the dendritic inhibition algorithm. Nodes are shown as large circles, excitatory synapses as small open circles and inhibitory synapses as small filled circles. Nodes  $Y_{1k}$  and  $Y_{3k}$  are selective for the double-width bars 1 and 3 respectively. The occurrence in an image of the double-width bar ‘bar 2’ would be indicated by both nodes  $Y_{1k}$  and  $Y_{3k}$  being active at half-strength. However, if bar 2 occurs sufficiently frequently, the negative afferent weights indicated will develop which will suppress this response and enable the uncommitted node ( $Y_{2k}$ ) to compete to respond to this pattern. Note that each bar would activate two columns each containing eight input nodes, but only one input node per column is shown for clarity.

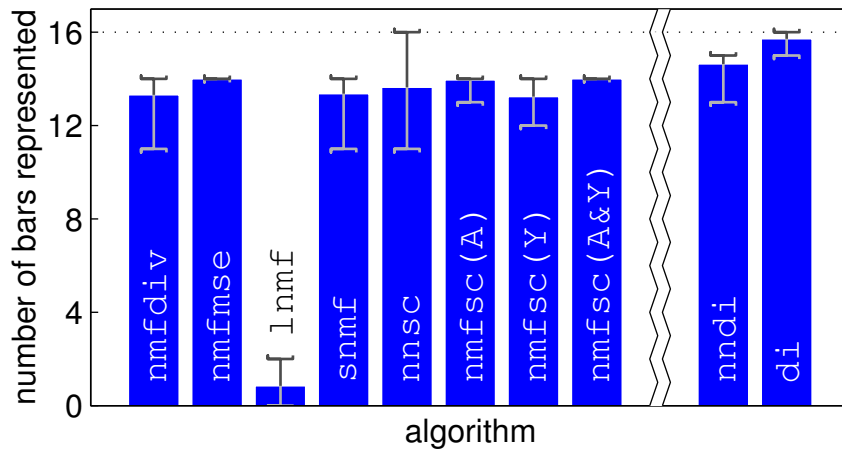


**Figure 10:** Performance of each algorithm when trained on the unequal bars problem, with 32 basis vectors or nodes, and  $p = 400$ . Each bar shows the mean number of components correctly identified by each algorithm when tested over 25 trials. Error bars show best and worst performance across the 25 trials.

the basis vectors (*i.e.*,  $\text{nmfsc}(A)$  and  $\text{nmfsc}(A \& Y)$ ) an alternative cause may be the imposition of a constraint that requires learnt image components to be a similar size, which is not the case for the components used in this task. The neural network algorithm with positive weights ( $\text{nndi}$ ) produced results that are only marginally better than the NMF algorithms. This algorithm also fails to reliably learn the two large components due to the large overlap between them. In contrast, the dendritic inhibition neural network algorithm with negative weights ( $\text{di}$ ), succeeded in identifying all the bars in most trials. As for the previous experiment with double-width bars, this result illustrates the need to allow negative weight values in this algorithm in order to robustly learn image components. Algorithm  $\text{di}$  learnt every image component in 18 of the 25 trials. In contrast, only one NMF algorithm ( $\text{nnsc}$ ) managed to find all the image components, but it only did so in a single trial.

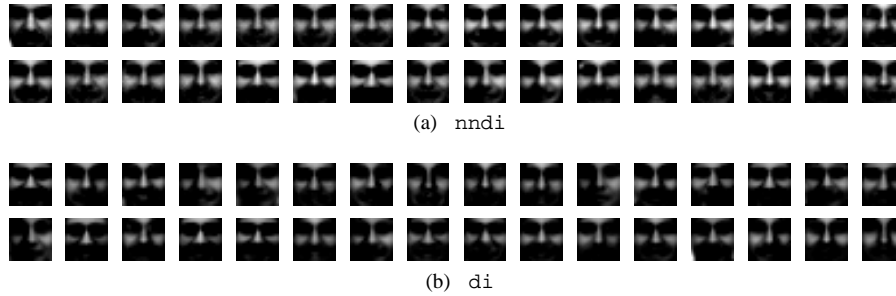


**Figure 11:** (a) and (b) Typical recognition weights learnt by 32 nodes when both versions of the dendritic inhibition algorithm were trained on the CBCL face database. Light pixels indicate strong weights.

### 3.5 Face Images

Previously, NMF algorithms have been tested using a training set that consists of images of faces (Lee and Seung, 1999; Hoyer, 2004; Li et al., 2001; Feng et al., 2002). When these training images are taken from the CBCL face database<sup>1</sup>, algorithm `nmfdi` learns basis vectors that correspond to localised image parts (Lee and Seung, 1999; Hoyer, 2004; Feng et al., 2002). However, when applied to the ORL face database<sup>2</sup>, algorithm `nmfmse` learns global, rather than local, image features (Li et al., 2001; Hoyer, 2004; Feng et al., 2002). In contrast, algorithm `lnmf` learns localised representations of the ORL face database (Feng et al., 2002; Li et al., 2001). Algorithm `nmfsc` can find either local or global representations of either set of face images with appropriate values for the constraints on the sparseness of the basis vectors and activations. Specifically, `nmfsc` learns localised image parts when constrained to produce highly sparse basis images, but learns global image features when constrained to produce basis images with low sparseness or if constrained to produce highly sparse activations (Hoyer, 2004). Hence, NMF algorithms can, in certain circumstances, learn localised image components, some of which appear to roughly correspond to parts of the face, but others of which are arbitrary, but localised, blobs. Essentially the NMF algorithms select a subset of the pixels which are simultaneously active across multiple images to be represented by a single basis vector. The same behaviour is observed in the bars problems, reported above, where a basis vector often corresponds to a random subset of pixels along a row or column of the image rather than representing an entire bar. Such arbitrary image components are not meaningful representations of the image data.

In contrast when the dendritic inhibition neural network is trained on face images, it learns global representations. Figure 11a and Figure 11b show the results of training `nndi` and `di`, for 10000 iterations, on the 2429 images in the CBCL face database. Parameters were identical to those used for the bars problems, except the weights were initialised to random values chosen from a Gaussian distribution with a larger standard deviation ( $0.005 \frac{n}{m}$ ) as this was found necessary to cause bifurcation of activity values. In both cases, each node has learnt to represent an average (or prototype) of a different subset of face images. When presented with highly overlapping training images the neural network algorithm will learn a prototype consisting of the common features between the different images (Spratling and Johnson, 2006). When presented with objects that have less overlap, the network will learn to represent the individual exemplars (Spratling and Johnson, 2006). These two forms of representation are believed to support perceptual categorisation and object recognition (Palmeri and Gauthier, 2004).

## 4 Discussion

The NMF algorithm `lnmf` imposes the constraint that the basis vectors be orthogonal. This means that image components may not overlap and, hence, results in this algorithm's failure across all versions of the bars task. In all these tasks the underlying image components are overlapping bars patterns (even if they do not overlap in any single training image, as is the case with the one-orientation bars problem).

NMF algorithms which find non-negative factors without other constraints (*i.e.*, `nmfdi` and `nmfmse`) generally succeed in identifying the underlying components of images when trained using images in which there is no occlusion (*i.e.*, on the linear and one-orientation bars problems). However, these algorithms fail when occlu-

<sup>1</sup>CBCL Face Database #1, MIT Center For Biological and Computation Learning, <http://www.ai.mit.edu/projects/cbcl>

<sup>2</sup>The ORL Database of Faces, AT&T Laboratories Cambridge, <http://www.cl.cam.ac.uk/Research/DTG/attarchive/facedatabase.html>

sion does occur between image components, and performance gets worse as the degree of occlusion increases. Hence, these algorithms fail to learn many image features in the standard bars problem and produce even worse performance when tested on the double-width bars problem.

NMF algorithms that find non-negative factors with an additional constraint on the sparseness of the activations (*i.e.*, `snmf`, `nnsc`, and `nmfsc(Y)`) require that the rows of  $\mathbf{Y}$  have a particular sparseness. Such a constraint causes these algorithms to learn components that are present in a certain fraction of the training images (*i.e.*, each factor is required to appear with a similar frequency). Such a constraint can overcome the problems caused by occlusion and enable NMF to identify components in training images where occlusion occurs. For example, `nnsc` produced good results on the double-width bars problem. Given sufficient training data, `nnsc` also reliably finds nearly all the image components in all experiments except for the standard bars test when  $n = 16$  and the unequal bars problem. However, `nmfsc(Y)` fails to produce consistently good results across experiments. This algorithm only reliably found all the image components for the standard bars problem when  $n = 16$  and for the linear bars problem. Despite constraining the sparseness of the activations, algorithm `snmf` produced poor results in all experiments except for the linear bars problem.

The NMF algorithm that finds non-negative factors with an additional constraint on the sparseness of the basis vectors (*i.e.*, `nmfsc(A)`) requires that the columns of  $\mathbf{A}$  have a particular sparseness. Such a constraint causes this algorithm to learn components that have a certain fraction of pixels with values greater than zero (*i.e.*, all factors are required to be a similar size). This algorithm produces good results across all the experiments except the unequal bars problem. Constraining the sparseness of the basis vectors thus appears to overcome the problems caused by occlusion and enable NMF to identify components in training images where occlusion occurs. However, this constraint may itself prevent the algorithm from identifying image components which are a different size from that specified by the sparseness parameter. The NMF algorithm that imposes constraints on both the sparseness of the activations and the sparseness of the basis vectors (*i.e.*, `nmfsc(A&Y)`) produces results similar to those produced by `nmfsc(A)`.

The performance of the `nmfsc` algorithm depends critically on the particular sparseness parameters that are chosen. As can be seen from figure 12, performance on a specific task can vary from finding every component in every trial, to failure to find even a single component across all trials. While appropriate values of sparseness constraint can enable the NMF algorithm to overcome inherent problems associated with the non-linear superposition of image components, inappropriate values of sparseness constraint will prevent the identification of factors that occur at a different frequency, or that are a different size, to that specified by the sparseness parameter chosen. This is particularly a problem when the frequency and size of different image components varies within a single task. Hence, the `nmfsc` algorithm was unable to identify all the components in the unequal bars problem with any combination of sparseness parameters (figure 12d). In fact, no NMF algorithm succeeded in this task: either because the linear NMF model could not deal with occlusion or because the algorithm imposed sparseness constraints that could not be satisfied for all image components.

The parameter search shown in figure 12 was performed in order to select the parameter values that would produce the best overall results across all the tasks used in this paper for algorithms `nmfsc(A)`, `nmfsc(Y)`, and `nmfsc(A&Y)`. However, in many real-world tasks the user may not know what the image components should look like, and hence, it would be impossible to search for the appropriate parameter values. The `nmfsc` algorithm is thus best suited to tasks in which all components are either a similar size or occur at a similar frequency, and for which this size/frequency is either known *a priori* or the user knows what the components should look like and is prepared to search for parameters that enable these components to be ‘discovered’ by the algorithm.

Sparseness constraints are also often employed in neural network algorithms. However, in such recognition models, sparseness constraints usually limit the number of nodes that are simultaneously active in response to an input image (Földiák and Young, 1995; Olshausen and Field, 2004). This is equivalent to constraining the sparseness in the *columns* of  $\mathbf{Y}$  (rather than the rows of  $\mathbf{Y}$ , or the columns of  $\mathbf{A}$ , as has been constrained in the NMF algorithms). Any constraints that impose restrictions on the number of active nodes will prevent a neural network from accurately and completely representing stimuli (Spratling and Johnson, 2004). Hence, such sparseness constraints should be avoided. The dendritic inhibition model succeeds in learning representations of elementary image features without such constraints. However, to accurately represent image features that overlap, it is necessary for negative weight values to be allowed. This algorithm (`di`) produced the best overall performance across all the experiments performed here. This is achieved because this algorithm does not falsely assume that image composition is a linear process, nor does it impose constraints on the expected size or frequency of occurrence of image components. The dendritic inhibition algorithm thus provides an efficient, on-line, algorithm for finding image components.

When trained on images that are composed of elementary features, such as those used in the bars problems, algorithm `di` reliably and accurately learns representations of the underlying image features. However, when trained on images of faces, algorithm `di` learns holistic representations. In this case, large subsets of the train-

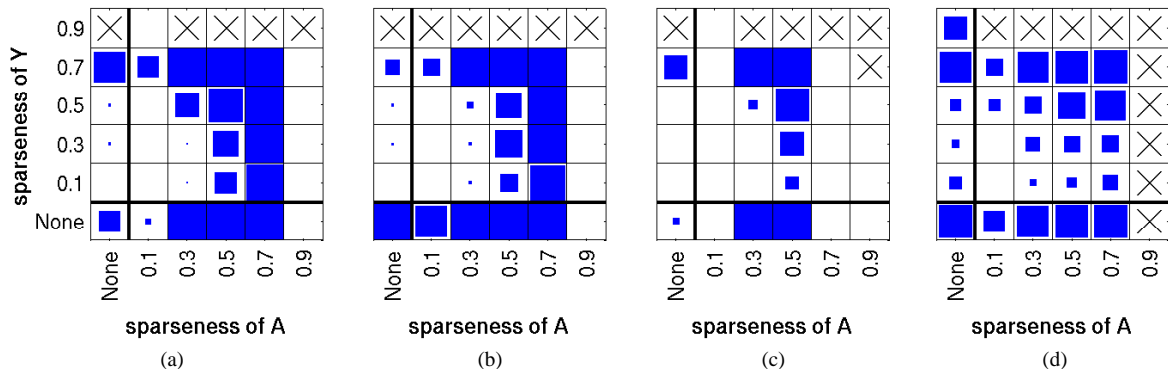


**Figure 12:** Performance of the `nmf_sc` algorithm across the range of possible combinations of sparseness parameters. For (a) the standard bars problem, (b) the one-orientation bars problem, (c) the double-width bars problem, and (d) the unequal bars problem. In each case,  $n = 32$  and  $p = 400$ . The sparseness of  $\mathbf{Y}$  varies along the y-axis and the sparseness of  $\mathbf{A}$  varies along the x-axis of each plot. Since the sparseness constraints are optional, 'None' indicates where no constraint was imposed. The length of the edge of each filled box is proportional to the mean number of bars learnt over 25 trials for that combination of parameters. Perfect performance would be indicated by a box completely filling the corresponding element of the array. 'X' marks combinations of parameter values for which the algorithm encountered a division-by-zero error and crashed.

ing images contain virtually identical patterns of pixel values. These re-occurring, holistic patterns, are learnt by the dendritic inhibition algorithm. In contrast, the NMF algorithms (in certain circumstances) form distinct basis vectors to represent pieces of these recurring patterns. The separate representation of sub-patterns is due to constraints imposed by the algorithms and is not based on evidence contained in the training images. Hence, while these constraints make it appear that NMF algorithms have learnt face parts, these algorithms are representing arbitrary parts of larger image features. This is demonstrated by the results generated when the NMF algorithms are applied to the bars problems. In these cases, each basis vector often corresponds to a random subset of pixels along a row or column of the image rather than representing an entire bar. Such arbitrary image components are not meaningful representations of the image data. Rather than relying on a subjective assessment of the quality of the components that are learnt, the bars problems that are the main focus of this paper, provide a quantitative test of the accuracy and reliability with which elementary image features are discovered. Since the underlying image components are known, it is possible to compare the components learnt with the known features from which the training images were created. These results demonstrate that when the training images are actually composed of elementary features, NMF algorithms can fail to learn the underlying image components, whereas, the dendritic inhibition algorithm reliably and accurately does so.

Intuitively, the dendritic inhibition algorithm works because the learning rule causes nodes to learn re-occurring patterns of pre-synaptic activity. As an afferent weight to a node increases, so does the strength with which that node can inhibit the corresponding input activity received by all other nodes. This provides strong competition for specific patterns of inputs and forces different nodes to learn distinct image components. However, because the inhibition is specific to a particular set of inputs, nodes do not interfere with the learning of distinct image components by other nodes. Unfortunately, the operation of this algorithm has not so far been formulated in terms of the optimisation of an objective function. It is hoped that the empirical performance of this algorithm will prompt the development of such a mathematical analysis.

## 5 Conclusions

Non-negative matrix factorisation employs non-negativity constraints in order to model the physics of image formation, and it has been claimed that this makes NMF particularly suited to learning meaningful representations of image data (Lee and Seung, 1999; Feng et al., 2002; Liu et al., 2003; Liu and Zheng, 2004; Li et al., 2001). However, by employing a linear model, NMF fails to take into account another important factor of image composition, namely the presence of occlusion. Hence, despite the claims, most NMF algorithms fail to reliably identify the underlying components of images, even in simple, artificial, tasks like those investigated here. These limitations can be overcome by imposing additional constraints on the sparseness of the factors that are found. However,

to employ such constraints requires *a priori* knowledge, or trial-and-error, to find appropriate parameter values and can result in failure to identify components that violate the imposed constraint. In contrast, a neural network algorithm, employing a non-linear activation function, can reliably and accurately learn image components. This neural network algorithm is thus more likely to provide a robust method of learning image components suitable for object recognition.

## Acknowledgements

This work was funded by the EPSRC through grant number GR/S81339/01. I would like to thank Patrik Hoyer for making available the MATLAB code that implements the NMF algorithms and which has been used to generate the results presented here.

## References

- Ahalt, S. C., Krishnamurthy, A. K., Chen, P., and Melton, D. E. (1990). Competitive learning algorithms for vector quantization. *Neural Networks*, 3:277–90.
- Barlow, H. B. (1990). Conditions for versatile learning, Helmholtz’s unconscious inference, and the task of perception. *Vision Research*, 30:1561–71.
- Barlow, H. B. (1995). The neuron doctrine in perception. In Gazzaniga, M. S., editor, *The Cognitive Neurosciences*, chapter 26. MIT Press, Cambridge, MA.
- Charles, D. and Fyfe, C. (1997). Discovering independent sources with an adapted PCA neural network. In Pearson, D. W., editor, *Proceedings of the 2nd International ICSC Symposium on Soft Computing (SOCO97)*. NAISO Academic Press.
- Charles, D. and Fyfe, C. (1998). Modelling multiple cause structure using rectification constraints. *Network: Computation in Neural Systems*, 9(2):167–82.
- Davies, G. M., Shepherd, J. W., and Ellis, H. D. (1979). Similarity effects in face recognition. *American Journal of Psychology*, 92:507–23.
- Dayan, P. and Zemel, R. S. (1995). Competition and multiple cause models. *Neural Computation*, 7:565–79.
- Feng, T., Li, S. Z., Shum, H.-Y., and Zhang, H. (2002). Local non-negative matrix factorization as a visual representation. In *Proceedings of the 2nd International Conference on Development and Learning (ICDL02)*, pages 178–86.
- Földiák, P. (1989). Adaptive network for optimal linear feature extraction. In *Proceedings of the IEEE/INNS International Joint Conference on Neural Networks*, volume 1, pages 401–5, New York, NY. IEEE Press.
- Földiák, P. (1990). Forming sparse representations by local anti-Hebbian learning. *Biological Cybernetics*, 64:165–70.
- Földiák, P. and Young, M. P. (1995). Sparse coding in the primate cortex. In Arbib, M. A., editor, *The Handbook of Brain Theory and Neural Networks*, pages 895–8. MIT Press, Cambridge, MA.
- Frey, B. J., Dayan, P., and Hinton, G. E. (1997). A simple algorithm that discovers efficient perceptual codes. In Jenkin, M. and Harris, L. R., editors, *Computational and Psychophysical Mechanisms of Visual Coding*. Cambridge University Press, Cambridge, UK.
- Fyfe, C. (1997a). Independence seeking negative feedback networks. In Pearson, D. W., editor, *Proceedings of the 2nd International ICSC Symposium on Soft Computing (SOCO97)*. NAISO Academic Press.
- Fyfe, C. (1997b). A neural net for PCA and beyond. *Neural Processing Letters*, 6(1-2):33–41.
- Ge, X. and Iwata, S. (2002). Learning the parts of objects by auto-association. *Neural Networks*, 15(2):285–95.
- Harpur, G. and Prager, R. (1996). Development of low entropy coding in a recurrent network. *Network: Computation in Neural Systems*, 7(2):277–84.
- Hinton, G. E., Dayan, P., Frey, B. J., and Neal, R. M. (1995). The wake-sleep algorithm for unsupervised neural networks. *Science*, 268(5214):1158–61.
- Hinton, G. E. and Ghahramani, Z. (1997). Generative models for discovering sparse distributed representations. *Philosophical Transactions of the Royal Society of London. Series B*, 352(1358):1177–90.
- Hochreiter, S. and Schmidhuber, J. (1999). Feature extraction through LOCOCODE. *Neural Computation*, 11:679–714.
- Hoyer, P. O. (2002). Non-negative sparse coding. In *Neural Networks for Signal Processing XII: Proceedings of the IEEE Workshop on Neural Networks for Signal Processing*, pages 557–65.
- Hoyer, P. O. (2004). Non-negative matrix factorization with sparseness constraints. *Journal of Machine Learning Research*, 5:1457–69.

- Jutten, C. and Herault, J. (1991). Blind separation of sources, part I: an adaptive algorithm based on neuromimetic architecture. *Signal Processing*, 24:1–10.
- Kohonen, T. (1997). *Self-Organizing Maps*. Springer-Verlag, Berlin.
- Lee, D. D. and Seung, H. S. (1999). Learning the parts of objects by non-negative matrix factorization. *Nature*, 401:788–91.
- Lee, D. D. and Seung, H. S. (2001). Algorithms for non-negative matrix factorization. In Leen, T. K., Dietterich, T. G., and Tresp, V., editors, *Advances in Neural Information Processing Systems 13*, Cambridge, MA. MIT Press.
- Li, S. Z., Hou, X., Zhang, H., and Cheng, Q. (2001). Learning spatially localized, parts-based representations. In *Proceedings of the IEEE Conference on Computer Vision and Pattern Recognition (CVPR01)*, volume 1, pages 207–12.
- Liu, W. and Zheng, N. (2004). Non-negative matrix factorization based methods for object recognition. *Pattern Recognition Letters*, 25(8):893–7.
- Liu, W., Zheng, N., and Lu, X. (2003). Non-negative matrix factorization for visual coding. In *Proceedings of the IEEE International Conference on Acoustics, Speech and Signal Processing (ICASSP03)*, volume 3, pages 293–6.
- Lücke, J. and von der Malsburg, C. (2004). Rapid processing and unsupervised learning in a model of the cortical macrocolumn. *Neural Computation*, 16(3):501–33.
- Meila, M. and Jordan, M. I. (2000). Learning with mixtures of trees. *Journal of Machine Learning Research*, 1:1–48.
- Oja, E. (1992). Principal components, minor components, and linear neural networks. *Neural Networks*, 5:927–35.
- Olshausen, B. A. and Field, D. J. (2004). Sparse coding of sensory inputs. *Current Opinion in Neurobiology*, 14:481–7.
- O’Reilly, R. C. (2001). Generalization in interactive networks: The benefits of inhibitory competition and Hebbian learning. *Neural Computation*, 13(6):1199–1242.
- Palmeri, T. J. and Gauthier, I. (2004). Visual object understanding. *Nature Reviews Neuroscience*, 5(4):291–303.
- Plumbley, M. D. (2001). Adaptive lateral inhibition for non-negative ICA. In *Proceedings of the international Conference on Independent Component Analysis and Blind Signal Separation (ICA2001)*, pages 516–21.
- Saund, E. (1995). A multiple cause mixture model for unsupervised learning. *Neural Computation*, 7(1):51–71.
- Sinha, P. and Poggio, T. (1996). I think i know that face.... *Nature*, 384(6608):404.
- Spratling, M. W. and Johnson, M. H. (2002). Pre-integration lateral inhibition enhances unsupervised learning. *Neural Computation*, 14(9):2157–79.
- Spratling, M. W. and Johnson, M. H. (2003). Exploring the functional significance of dendritic inhibition in cortical pyramidal cells. *Neurocomputing*, 52-54:389–95.
- Spratling, M. W. and Johnson, M. H. (2004). Neural coding strategies and mechanisms of competition. *Cognitive Systems Research*, 5(2):93–117.
- Spratling, M. W. and Johnson, M. H. (2006). A feedback model of perceptual learning and categorisation. *Visual Cognition*, 13(2):129–65.